Dynamics of Forebody Flow Separation and Associated Vortices

L. E. Ericsson* and J. P. Reding†
Lockheed Missiles and Space Company, Inc., Sunnyvale, California

It is well established that there is a strong coupling between body motion and boundary layer separation with attendant vortex shedding. In the present paper this coupling is studied for the particular case of a missile or an aircraft fuselage at very high angles of attack. It is shown that the unusual results obtained in recent tests can be explained by considering the so-called "moving-wall effect" on boundary layer transition and/or separation.

Nomenclature

b = wing span
c = reference length, mean chord for wing body, maximum diameter (d) for body alone
d = cylinder diameter
ℓ' = rolling moment: coefficient $C_\ell = \ell'/(\rho_\infty U_\infty^2/2)Sb$
ℓ = sectional lift: coefficient $c_\ell = \ell/(\rho_\infty U_\infty^2/2)c$
l = body length
M_p = pitching moment: coefficient $C_m = M_p/(\rho_\infty U_\infty^2/2)Sc$
N = normal force: coefficient $C_N = N/(\rho_\infty U_\infty^2/2)S$
n = yawing moment: coefficient $C_n = n/(\rho_\infty U_\infty^2/2)Sb$
p = spin rate
q = pitch rate
Re = Reynolds number, $Re = U_\infty d/\nu_\infty$
S = reference area, wing area or maximum cross-sectional area
t = time
U = velocity
x = distance from nose tip
Y = side force: coefficient $C_Y = Y/(\rho_\infty U_\infty^2/2)S$
α = angle of attack
β = angle of side slip
ν = kinematic viscocity of air
ρ = air density
φ = meridional coordinate
ϕ = coning angle

Subscripts

N = nose tip
W = wall
∞ = freestream conditions

Differential Symbols

$\dot{\phi} = \partial\phi/\partial t$
$\ddot{\phi} = \partial^2\phi/\partial t^2$
$C_{nq} = \partial C_n/\partial\left(\frac{cq}{U_\infty}\right)$
$C_{m\dot{\alpha}} = \partial C_m/\partial\left(\frac{c\dot{\alpha}}{U_\infty}\right)$

Presented as Paper 83-2118 at the AIAA Atmospheric Flight Mechanics Conference, Gatlinburg, Tenn., Aug. 15-17, 1983; received Sept. 15, 1983; revision received Feb. 16, 1984.

*Senior Consulting Engineer. Fellow AIAA.
†Staff Engineer. Associate Fellow AIAA.

Introduction

CONTINUALLY increasing performance demands have created a need to understand vehicle aerodynamics at high angles of attack,[1-3] where separated flow and associated vortices often have a dominating influence.[4-6] In the present paper the strong coupling between body motion and separated flow vortices is analyzed, showing how the so-called "moving-wall" effects can explain apparently anomalous results obtained in recent dynamic tests.

Magnus Lift

The classic Magnus lift characteristics of a rotating circular cylinder represent a pure case of moving-wall effects.[7,8] The wall-jet-like effect of the moving wall[7] is illustrated in Fig. 1 for the case $U_W/U_\infty = 1$. On the top side, downstream moving-wall effects fill out the velocity profile, thereby delaying flow separation, whereas on the bottom half, upstream moving-wall effects have the opposite effect, promoting flow separation. The upstream moving-wall effects are by far the strongest as is demonstrated by comparing the experimental Magnus lift for laminar (Fig. 2) and turbulent (Fig. 3) flow conditions.[7] (This nomenclature refers to the initial boundary-layer conditions existing at $p = 0$.) In the laminar case, the Magnus lift is generated mainly by the downstream moving-wall effect on the top side, moving the separation from the subcritical towards the supercritical position (Fig. 1). On the bottom side, the separation is already of the subcritical type $p = 0$, and the upstream moving-wall effect does not have much leverage for its separation-promoting action. In the turbulent case (Fig. 2), however, the situation is reversed. The main effect is that of the upstream moving-wall on the bottom side, promoting separation, moving it from the supercritical towards the subcritical position. The difference in Magnus lift slope, $\partial c_\ell/\partial(U_W/U_\infty) = 0.75$ for laminar flow vs the turbulent value of $\partial c_\ell/\partial(U_W/U_\infty) = 2.2$, reflects the fact that the adverse upstream moving-wall effect dominates.

These moving-walls effects on flow separation are rather straightforward and explain the positive Magnus lift slopes, $\partial c_\ell/\partial(U_W/U_\infty) > 0$. The negative slopes, $\partial c_\ell/\partial(U_W/U_\infty) < 0$, occurring at a critical wall velocity must also be considered, however. The so-called Magnus lift reversals are caused by the moving-wall effect on boundary-layer transition. In the laminar case (Fig. 1), when $p > p_{crit}$, the upstream moving-wall effect on the bottom side causes boundary-layer transition to occur before separation, changing it from the subcritical towards the supercritical type. This effect completely overpowers the regular moving-wall effects and causes a more or less discontinuous loss of lift (Fig. 2). In the turbulent case (Fig. 3) it is the downstream moving-wall effect on the top side that delays transition, causing it to move downstream of the separation point, thereby changing the

separation from the supercritical towards the subcritical type, again generating a discontinuous loss of lift.

In both cases of Magnus lift reversal just discussed, the changes were towards, but not all the way to, the subcritical or supercritical separation types, the full change being restricted by the "regular" moving-wall effects. However, at critical flow conditions these restrictions are no longer present, and negative lift is generated immediately when p changes from $p=0$ to $p>0$ (Fig. 4). Thus, the wall velocity need not reach a certain magnitude before Magnus lift reversal occurs, as was the case for laminar and turbulent initial flow conditions (Figs. 2 and 3). The effect is very similar to the effect of Reynolds number on transitional flow separation, with the downstream/upstream moving-wall effect corresponding to the effect of decreasing/increasing Reynolds number. Thus, the flow separation extent increases on the top side and decreases on the bottom side, generating the negative lift shown in Fig. 3.

High-α Aerodynamics

The moving-wall effects on slender bodies of revolution at high angles of attack have a great deal in common with the two-dimensional effects shown in Figs. 1-4. Test results for an ogive-cylinder with a spinning nose tip[10] give a very vivid demonstration of how powerful the moving-wall effects can be (Fig. 5). At $\alpha=55$ deg the flow conditions on the nose tip apparently were of the critical type shown in Fig. 4. Thus, it is the direction, rather than the rate of the spin, that determines the vortex-induced side force. The data also show a spin rate hysteresis effect, as has been measured by others[11] and can be expected, based upon observed Reynolds number hysteresis. The critical condition shown in Fig. 4 can also be realized by an ogive-cylinder in the pitchup motion[12] (Fig. 6). The very modest pitch rate of $\dot{\alpha}d/U_\infty=0.0027$ changes the supercritical separation existing at $\dot{\alpha}=0$ for $Re=0.08\times10^6$ to the subcritical type existing at $\dot{\alpha}=0$ and $Re=0.05\times10^6$ (the quoted 6% oscillatory variation of the freestream speed may have been responsible for this early subcritical/supercritical transition). The change is caused by the downstream moving-wall effect on transition shown in Fig. 3, which delays transition and causes a change from supercritical towards subcritical separation. It is discussed in Ref. 4 how heretofore unexplained data trends for coning bodies[13,14] also can be explained by the moving-wall effects illustrated in Figs. 2 and 3.

Recent test results[15] illustrate how powerful the moving-wall effects are on a cone-cylinder body at laminar flow conditions (Fig. 7). The authors describe how only a slight push was needed to establish the coning motion in one direction or the other, regardless of the fact that the measured static side force was biased in one direction due to nose microasymmetries.[5,6] The body reached very nearly equal steady state coning rates in positive and negative rotation directions (Fig. 7). That is, the motion dominated over the static asymmetry, locking in the vortex asymmetry in the direction of the body motion. A mechanism that can cause this lock-in of the vortex asymmetry is the moving-wall effect described earlier for the rotating cylinder (Figs. 2 and 3). In the case of a coning motion the situation is as sketched in Fig. 8. The lateral motion of the circular cross-section causes the

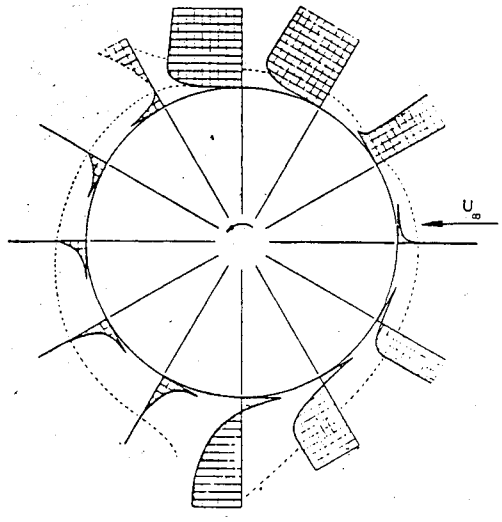

Fig. 1 Computed boundary layer flow profiles on a rotating circular cylinder with $U_w=U_\infty$ (Ref. 7).

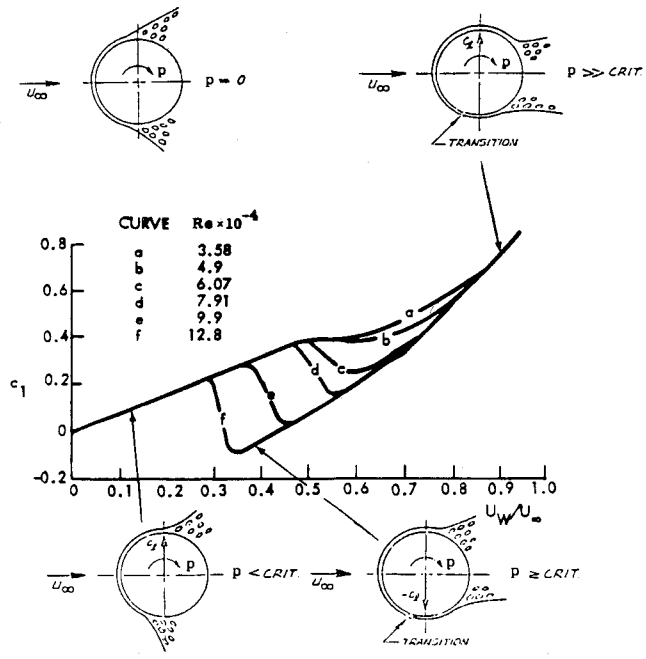

Fig. 2 Moving wall effects on a rotating circular cylinder with laminar initial flow conditions.

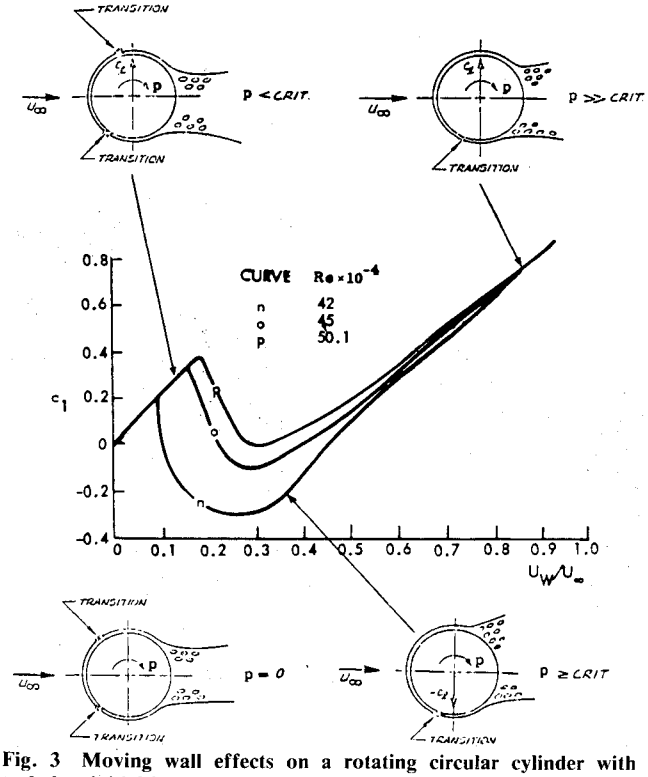

Fig. 3 Moving wall effects on a rotating circular cylinder with turbulent initial flow conditions.

flow separation to be delayed on the advancing side and promoted on the retreating side due to moving-wall effects very similar to those discussed in Figs. 2 and 3. Thus, the motion generates a force that drives it until the equilibrium coning rate is reached (Fig. 7). This limiting rate could be established in a manner similar to that for the limit cycle amplitude for an oscillating circular cylinder in two-dimensional flow. That is, the driving or undamping coning moment due to the flow separation asymmetry is balanced by the damping drag moment. According to the two-dimensional analogy, the local, sectional driving force would be proportional to the product of the stream velocity and the coning rate, whereas the damping drag force should become proportional to the square of the rate for high coning rates. This would result in a linear growth of the equilibrium coning rate with increasing freestream velocity in agreement with the data trend in Fig. 7. The three-dimensionality and combined effects of moving-wall velocity and Reynolds number can probably explain the deviations in Fig. 7 from this expected local, sectional data trend.

The flow visualization results[15] in Fig. 9 indicate that two sets of asymmetric vortices exist on the cone cylinder body at the incipient coning conditions for $\alpha = 45$ deg shown in Fig. 7. With $l/d = 5.5$ and a blunted conic nose tip, the cone-cylinder would be expected to have only one vortex pair at $\alpha = 45$ deg in a static test.[5,6] The authors state in Ref. 15 that at rest one pair of almost symmetrical vortices were indeed observed. The moving-wall effect illustrated in Fig. 8a promotes the asymmetric separation and vortex formation on the coning body.

Thus, the coning blunted cone-cylinder behaves similarly to a pointed cone- or ogive-cylinder body in steady flow. For the slightly subcritical test conditions, the minimum cell length of

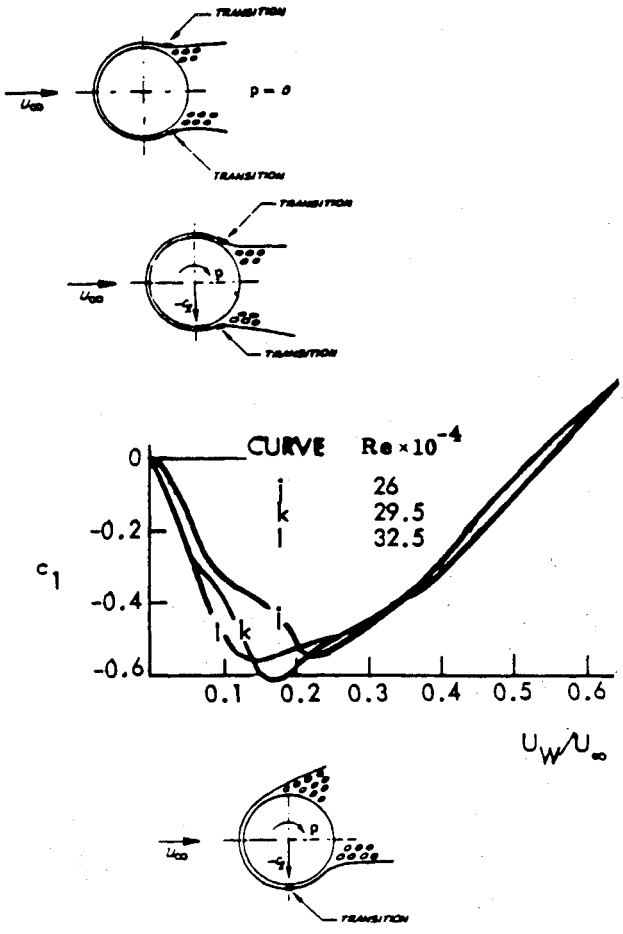

Fig. 4 Moving wall effects on a rotating circular cylinder at critical flow conditions.

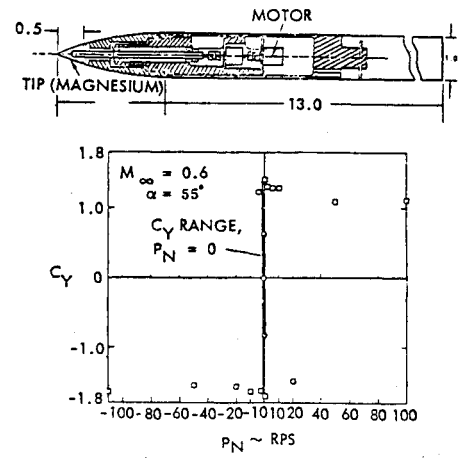

Fig. 5 Effect of spinning nose tip on vortex-induced side force at $\beta = 0$ (Ref. 10).

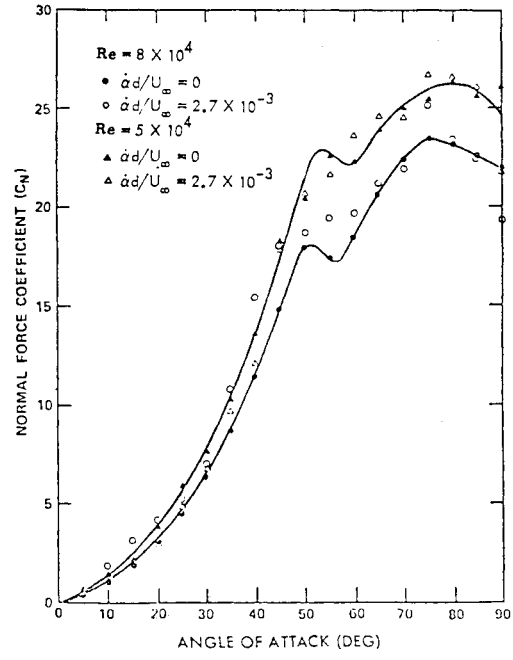

Fig. 6 Pitch rate effect on ogive-cylinder normal force at critical flow conditions (Ref. 12).

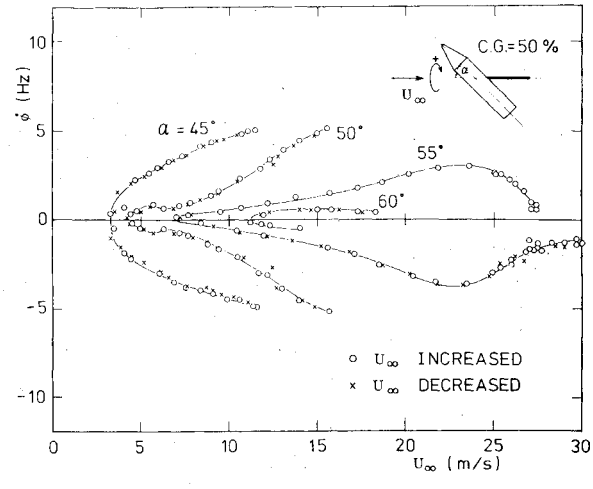

Fig. 7 Coning characteristics of a cone-cylinder at $\alpha \leq 60$ deg. (Ref. 15).

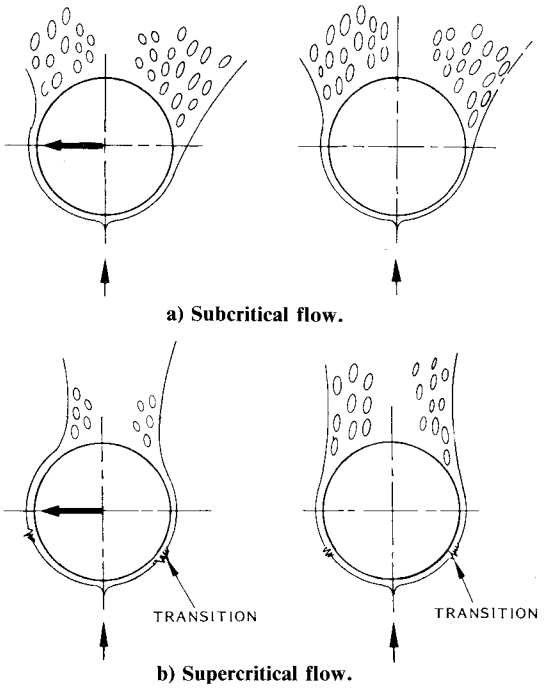

Fig. 8 Effect of coning motion on flow separation asymmetry.

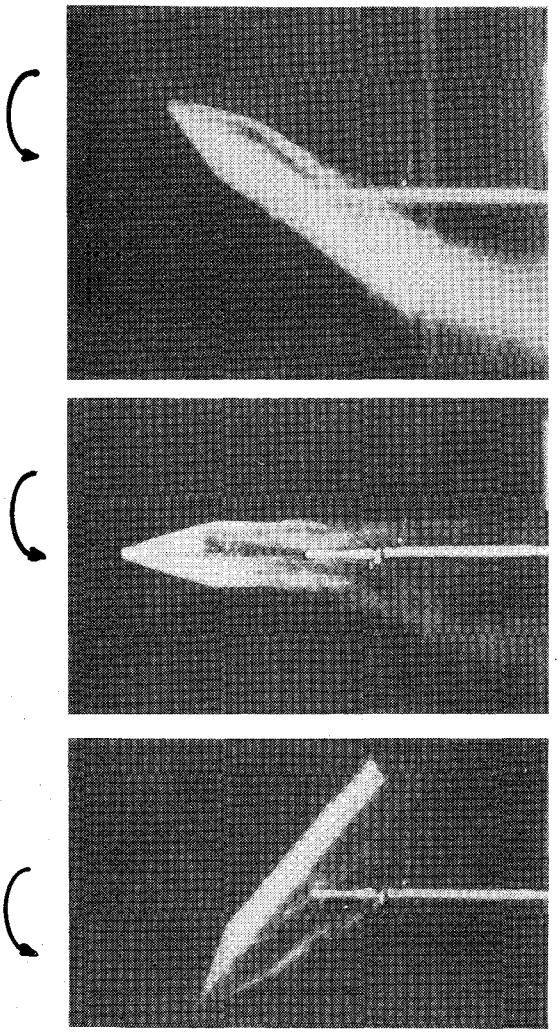

Fig. 9 Smoke flow pictures of a cone-cylinder at incipient coning conditions, $\alpha = 45$ deg, $U_\infty \approx 3.5$ m/s (Ref. 15): a) two sets of vortices on both sides of the body; b) vortices are shifted on the nose and downstream; c) two sets of asymmetric vortices exist.

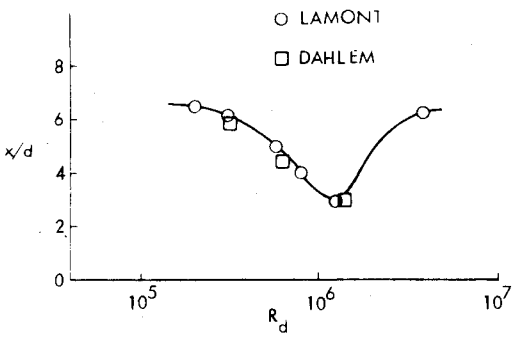

Fig. 10 Contraction of the first asymmetric vortex cell in the critical Reynolds number region (Ref. 16).

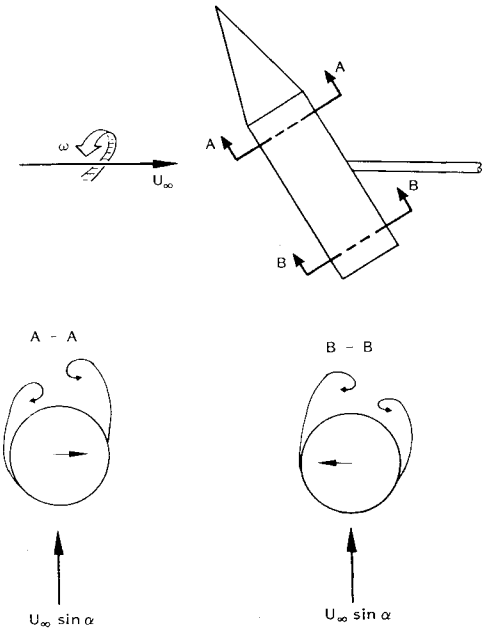

Fig. 11 Fore- and aft body flow separation asymmetry on a cone-cylinder coning at $\alpha = 45$ deg.

$x/d = 2.5$ for the first asymmetric vortex pair would be approached[16] (Fig. 10). Consequently, the vortex on the "coning leeside" (Fig. 8a) should lift off before the rotation center at $x/d = 2.75$ on the cone-cylinder in Fig. 3. As a consequence the opposite vortex asymmetry would develop aft of the rotation center, resulting in the force-couple type of load conditions illustrated in Fig. 11. This is also the loading measured at $\alpha = 90$ deg where in absence of motion the separation asymmetry oscillates in response to the unsteady Karman vortex shedding. As in the case of the rotating cylinder (Figs. 1-4) the translatory motion for a cylinder, coning at high angles of attack (Fig. 8), should generate a time-average-separation asymmetry that drives the coning motion[17] (Fig. 12).

The pressure distribution data show how the downstream moving-wall effect on the advancing side causes the separation to be of the critical (laminar bubble) type, which generates the highest suction peak,[16] whereas the upstream moving-wall effect on the retreating side promotes a subcritical type of separation. The advancing side is identified by the skewed stagnation pressure peak, at $\varphi \approx 20$ deg rather than at $\varphi = 0$. The pressure distribution between $\varphi = 20$ deg and $\varphi = 160$ deg is typical for critical flow conditions,[16] whereas the pressures between $\varphi = 270$ deg and $\varphi \approx 340$ deg signify subcritical type laminar flow separation. The subcritical-critical flow separation asymmetry results in large pressure differentials in the vicinity of the lateral meridians, $\varphi = 90$ deg

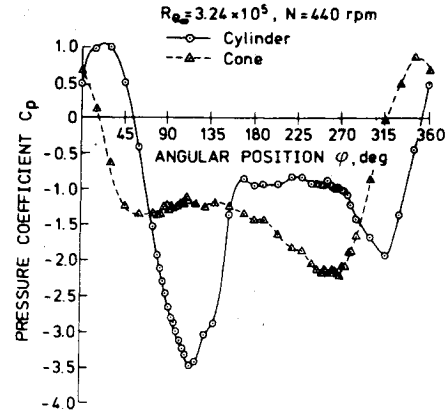

Fig. 12 Pressure distribution on a cylinder and a cone-cylinder coning at $\alpha = 90$ deg (Ref. 17).

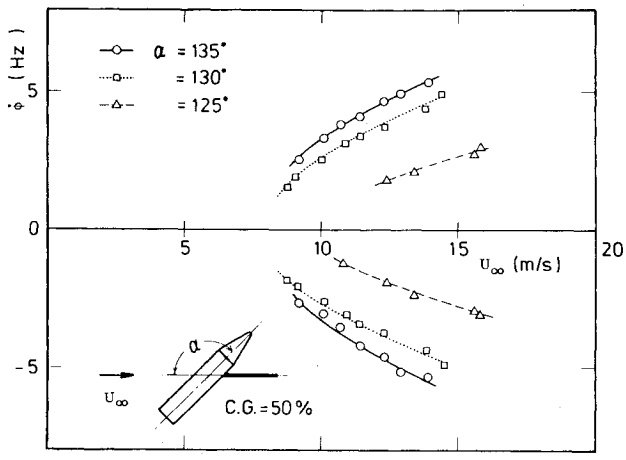

Fig. 13 Coning rates of cone-cylinder at $\alpha > 90$ deg (Ref. 15).

and $\varphi = 270$ deg, generating a force that drives the motion. On the conic nose a similar driving side force is generated, although of less magnitude. The results in Fig. 12 support the conclusions drawn in Refs. 4 and 16 that body motion can lock in the flow asymmetry that results in the maximum side force.

At first the results for the coning cone-cylinder body in Fig. 9 appear to contradict the results obtained by Tobak et al.,[13] which showed that the skewing of a symmetric vortex pair, generated on the slender conic nose, does not switch bias (or sign) aft of the rotation center. However, in the case of the symmetric vortex pair, no lift-off occurs, and the moving-wall effects can affect only the vortex formation on the nose. Once established, the vortices do not react to moving-wall effects further downstream, unless a condition of lift-off is approached. Lift-off of the other forebody vortex might be caused by the support.[18,19] Although the sting is very slender, the remaining forebody vortex is not only closer to the surface than the one lifting off, but is also close to the centerline of the body (see later discussion of Fig. 17).‡ If both vortices lift off, local aft body moving-wall effects will dictate the formation of a new vortex pair.

When the cone-cylinder body was turned around, exposing the flat-faced cylinder to the air stream, a similar type of

‡After the publication of this paper in preprint form,[20] Yoshinaga informed us "As we have some worries about the effect of the sting to which the vortex collided some time in the coning experiments, we are intending to make experiments again by changing the supporting method."[21]

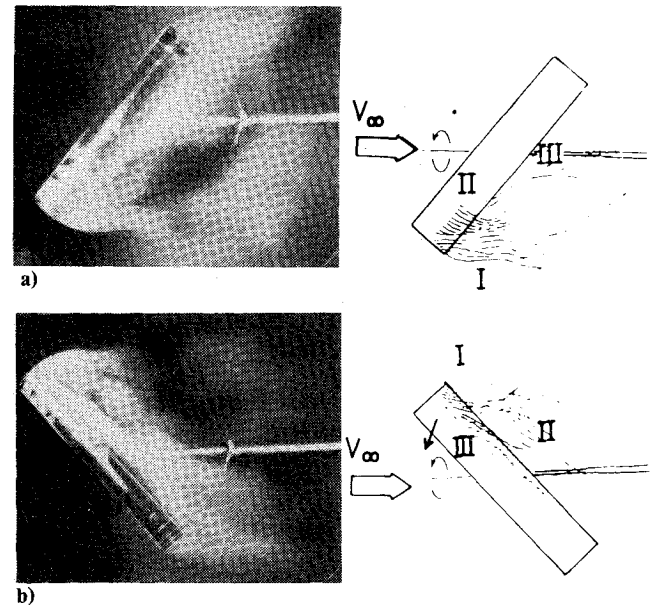

Fig. 14 Smoke flow pictures of flat-faced circular cylinder coning at $\alpha = 50$ deg (Ref. 15): a) separated side (II); b) reattached side (III).

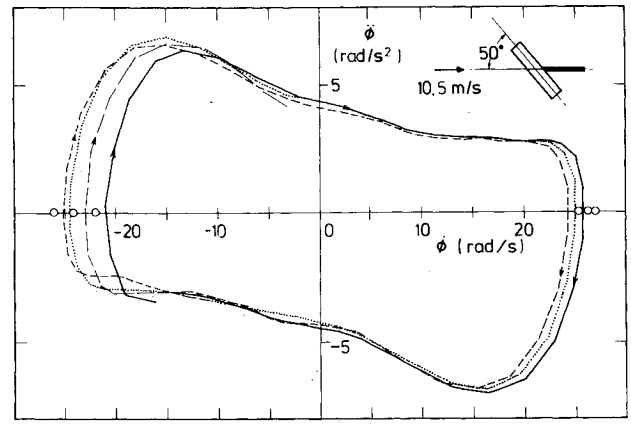

Fig. 15 Acceleration-rate time history for a flat-faced circular cylinder coning at $\alpha = 50$ deg. (Ref. 15).

mirror-symmetric equilibrium coning rates was measured[15] (compare Figs. 7 and 13). However, in this case no exterior push was needed to change the direction of the coning. Movies taken of a flat-faced cylinder at $\alpha = 50°$ (Fig. 14) showed that the cylinder area immediately aft of the three-dimensional, nose-induced flow separation, generated on bluff noses,[22-24] had reattached flow behavior on the advancing side of the body, which will produce a driving suction force (see Fig. 8a). The associated accelerations and coning rates are shown in Fig. 15. It can be seen that when a limiting coning rate is reached the acceleration suddenly switches sign. The coning rate is steadily decreasing, passing through zero, until its limit on the opposite side is reached and the acceleration switches sign again. This is repeated cycle after cycle with some scatter in the limiting rates (Fig. 16).

The behavior described above can be explained by the moving-wall effects on transitions, which caused the Magnus lift reversal in Fig. 2 for the subcritical conditions applicable here (Fig. 16). In the right-hand sketch the initial subcritical separation asymmetry is shown. This generates a side force that drives the cross-section to the left with a driving force that increases with increasing translatory velocity (Fig. 8a). (In addition, the acceleration is affected by the drag-damping discussed earlier.) When a critical value of the coning rate is

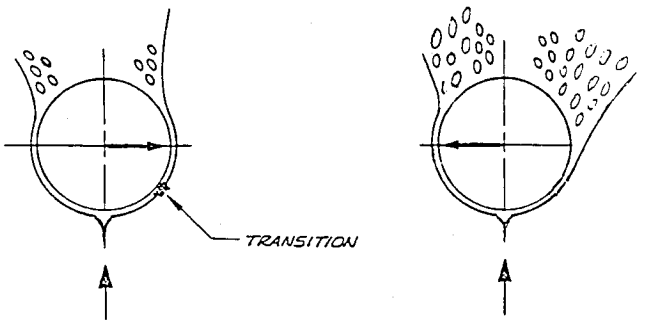

Fig. 16 Effect of coning motion on flow separation asymmetry at slightly subcritical initial conditions.

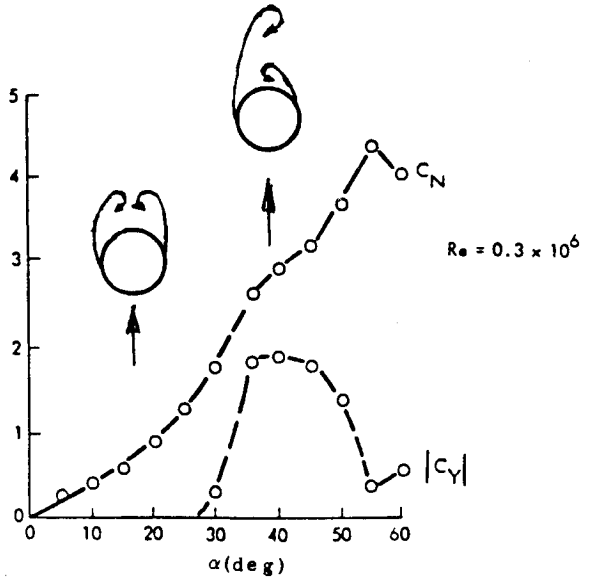

Fig. 17 Correlation of vortex-induced effects on $C_N(\alpha)$ and $C_Y(\alpha)$ of an $l/d=5$ tangent-ogive at $\beta=0$. (Ref. 27).

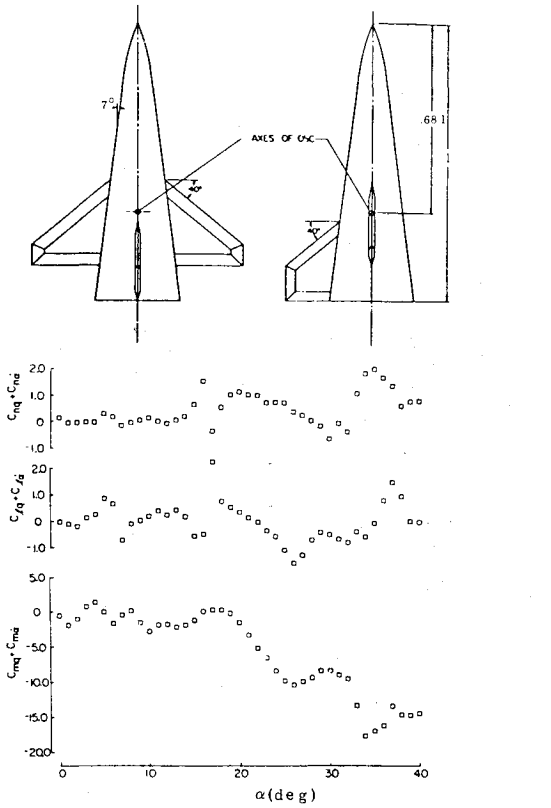

Fig. 18 Pitch-induced dynamic derivatives at $M_\infty=0.7$ and $\beta=5$ deg. (Ref. 28).

reached, the upstream moving-wall effect will cause transition to occur on the receding side of the cylinder. The associated switch from subcritical to supercritical type flow separation would cause a large discontinuous change of the force in the opposite direction (Fig. 2), resulting in a reversal of the driving force for the coning body (Fig. 16). Once established in the opposite direction, the asymmetry has a certain inertia, resulting in rate hysteresis. That is, transition does not disappear back into the wake immediately when the coning rate is decreased.

When transition finally is "swallowed" by the wake, the asymmetry, now for laminar flow conditions, will remain of the same bias, driving the rate of coning motion through zero up to the limiting value in the other direction, when the mirror symmetry of the change shown in Fig. 16 will take place and a new cycle of the oscillatory coning is started. A similar type of behavior can be expected at supercritical initial flow conditions,[20] when the downstream moving-wall effect causes transition to move downstream of the separation, resulting in an even larger reversal of the side force and Magnus lift (Fig. 3). As the freestream velocity, and thereby the Reynolds number, was increased, the angular rate at which the "flipping" of the separation asymmetry occurred increased also[15] (Fig. 13), in agreement with the data trends for the Magnus lift (Fig. 2).

The acceleration-rate characteristics for the cone-cylinder "flying backwards" are very similar to those for the cylinder alone,[15] indicating that only one set of asymmetric vortices are generated with associated forebody dominance, contrary to the results discussed earlier for the nose-first orientation of the cone-cylinder body (Figs. 9 and 11). This result is in basic agreement with the delayed asymmetry development with increasing nose bluntness.[6,19] The lack of symmetry (the skewness) of the loops in Fig. 15 could be caused by the model support irregularities discussed by the authors,[15] which made the coning angle larger in the clockwise than in the anticlockwise direction.

Vortex-Induced Downstream Loads

The body vortices, which are generated by upstream flow separation, will generate significant loads on the downstream body, wing, and tail surfaces.[25] Even a symmetric vortex pair can, through its entrainment effect, create a highly nonuniform flow field at the tail.[26] When the vortices turn asymmetric at higher angles of attack, the vortex remaining close to the body moves inboard, generating an increase of the lift instead of the otherwise expected decrease, caused by the lift-off of one vortex[5,6,27] (Fig. 17). This single vortex dominance can explain the dramatic vortex-induced nonlinear effect on the yaw-pitch cross-coupling derivatives measured by Orlik-Rückemann[28] (Fig. 18). These vortex-induced loads can be distorted in wind tunnel tests by the interference from the support system.[18]

Conclusions

A review and further analysis of recent experimental results for the high-α vehicle dynamics of axisymmetric bodies has shown the following:

1) The coupling between vehicle motion and asymmetric forebody flow separation with attendant vortices is extremely strong, easily overpowering any existing static asymmetry, making it possible for a maneuvering vehicle to experience especially large asymmetric loads.

2) The observed coupling can be explained by the moving-wall effects previously demonstrated in the case of Magnus lift generation.

3) In regard to downstream effects of the separated flow vortices, they can become much more severe when the vortices become asymmetric, since this leaves one vortex close to the body-surface near the centerline with resulting interference effects on a downstream fin, generating large static and dynamic cross-coupling effects.

References

[1] "Dynamic Stability Parameters," AGARD CP-235, Nov. 1978.

[2] Ericsson, L. E., "Technical Evaluation Report on the Fluid Dynamics Panel Symposium on Dynamic Stability Parameters," AGARD-AR-137, April 1979.

[3] Ericsson, L. E., "A Summary of AGARD FDP Meeting on Dynamic Stability Parameters," Paper 2, AGARD CP-260, May 1979.

[4] Ericsson, L. E. and Reding, J. P., "Steady and Unsteady Vortex-Induced Asymmetric Loads on Slender Vehicles," *Journal of Spacecraft and Rockets,* Vol. 18, March/April, 1981, pp. 97-109.

[5] Ericsson, L. E. and Reding, J. P., "Review of Vortex-Induced Asymmetric Loads—Part I," *Zeitschrift für Flugwisseuschaften und Weltraumforschung* (1981) Heft 3, pp. 162-174.

[6] Ericsson, L. E. and Reding, J. P., "Review of Vortex-Induced Asymmetric Loads—Part II," *Zeitschrift für Flugwisseuschraften und Weltraumforschung* (1981) Heft 6, pp. 349-366.

[7] Swanson, W. M., "The Magnus Effect: A Summary of Investigations to Date," *Journal of Basic Engineering,* Vol. 83, Sept. 1961, pp. 461-470.

[8] Ericsson, L. E., "Karman Vortex Shedding and the Effect of Body Motion," *AIAA Journal,* Vol. 18, Aug. 1980, pp. 935-944.

[9] Chapman, D. R., "Kuehn, D. M., and Larson, H. K., "Investigation of Separated Flow on Supersonic and Subsonic Streams with Emphasis on the Effect of Transition," NACA TN-3869, March 1957.

[10] Fidler, J. E., "Active Control of Asymmetric Vortex Effects," *Journal of Aircraft,* Vol. 18, April 1981, pp. 267-272.

[11] Malcolm, G. N. and Clarkson, M. H., "Wind Tunnel Testing with a Rotary-Balance Apparatus to Simulate Aircraft Spin Motions," *Proceedings of AIAA 9th Aerodynamic Testing Conference,* Arlington, Tex., June 1976, pp. 143-146.

[12] Smith, L. H., "Aerodynamic Characteristics of Axisymmetric Body Undergoing a Uniform Pitching Motion," Ph.D. Thesis, Naval Post-Graduate School, Monterey, Calif., Dec. 1974.

[13] Tobak, M., Schiff, L. B., and Peterson, V. L., "Aerodynamics of Bodies of Revolution in Coning Motion," *AIAA Journal,* Vol. 7, Jan. 1969, pp. 95-99.

[14] Schiff, L. B. and Tobak, M., "Results from a New Wind-Tunnel Apparatus for Studying Coning and Spinning Motions of Bodies of Revolution," *AIAA Journal,* Vol. 8, Nov. 1970, pp. 1953-1958.

[15] Yoshinaga, T., Tate, A., and Inoue, K., "Coning Motion of Slender Bodies at High Angles of Attack in Low Speed Flow," AIAA Paper 81-1899, Aug. 1981.

[16] Reding, J. P. and Ericsson, L. E., "Re-examination of the Maximum Normalized Vortex—Induced Side Force," *Journal of Spacecraft and Rockets,* Vol. 21, Sept./Oct. 1984, pp. 433-440.

[17] Kubota, H., Arai, I., and Matsuzaka, M., "Flat Spin of Slender Bodies at High Angles of Attack," *Journal of Spacecraft and Rockets,* Vol. 20, March/April 1983, pp. 108-114.

[18] Ericsson, L. E. and Reding, J. P., "Review of Support Interference in Dynamic Tests," *AIAA Journal,* Vol. 21, Dec. 1983, pp. 1652-1666.

[19] Ericsson, L. E. and Reding, J. P., "Alleviation of Vortex-Induced Asymmetric Loads," *Journal of Spacecraft and Rockets,* Vol. 17, Nov./Dec. 1980, pp. 546-553.

[20] Ericsson, L. E. and Reding, J. P., "Dynamics of Forebody Flow Separation and Associated Vortices," AIAA Paper 83-2118, Aug. 1983.

[21] Yoshinaga, T., Private Communication, Dec. 28, 1983.

[22] Ericsson, L. E., "Unsteady Aerodynamic of Separating and Reattaching Flow on Bodies of Revolution," *Recent Research on Unsteady Boundary Layers,* Vol. 1, International Union of Theoretical and Applied Mechanics Symposium, Laval University, Quebec, Canada, May 24-28, 1971, pp. 481-512.

[23] Hall, I. M., Rogers, E. W. E., and Davies, B. M., "Experiments With Inclined Blunt-Nosed Bodies at M = 2.45," ARC R & M No. 3128, Aeronautical Research Council, Great Britain, August 1957.

[24] Ericsson, L. E. and Reding, J. P., "Vortex-Induced Asymmetric Loads on Slender Vehicles," LMSC-D630807, Lockheed Misiles and Space Company, Inc., Sunnyvale, Calif., Jan. 1979.

[25] Ericsson, L. E. and Reding, J. P., "Effect of Flow Separation Vortices on Aircraft Unsteady Aerodynamics," Paper 24, AGARD CP-235, May 1978.

[26] Reding, J. P. and Ericsson, L. E., "Review of Delta Wing Space Shuttle Vehicle Dynamics," *Proceedings Space Shuttle Aerothermodynamics Conference,* Vol. III, (NASA TMX-2508). NASA Ames RC, Moffett Field, Calif. Dec. 15-16, 1971, pp. 861-931.

[27] Keener, E. R., Chapman, G. T., Cohen, L., and Taleghani, J., "Sides Forces on Forebodies at High Angles of Attack and Mach Numbers from 0.1 to 0.7. Two Tangent Ogives, Paraboloid and Cone," NASA TMX-3438, Feb. 1977.

[28] Orlik-Rückemann, K. J., "Aerodynamic Coupling Between Lateral and Longitudinal Degrees of Freedom," *AIAA Journal,* Vol. 15, Dec. 1977, pp. 1792-1799.